# Peptide-Mediated Cell Transport of Water Soluble Porphyrin Conjugates

Martha Sibrian-Vazquez, Timothy J. Jensen, Robert P. Hammer, and M. Graça H. Vicente*

*Department of Chemistry, Louisiana State University, Baton Rouge, Louisiana 70803*

Five new porphyrin−peptide conjugates bearing a nuclear localizing sequence SV40 or a fusogenic peptide (HIV-1Tat 40−60 or octa-arginine) linked by low molecular weight poly(ethylene glycol) have been synthesized. In vitro studies using human HEp2 cells show that the cellular uptake of the conjugates depends significantly on the nature and sequence of amino acids in the peptide and on the nature of the substituents on the porphyrin macrocycle. The fusogenic peptide sequences HIV-1Tat 40−60 and octa-arginine were the most effective in delivering the conjugates to the cells. The subcellular distribution of the conjugates was found to be dependent on the nature of substituents on the porphyrin macrocycle. The conjugates bearing a hydrophobic porphyrin localized preferentially in the endoplasmic reticulum and were significantly more phototoxic to HEp2 cells than the carboxylic acid functionalized porphyrin conjugates, which localized mainly in the lysosomes.

## Introduction

The biological efficacy of porphyrin-based sensitizers for the photodynamic therapy (PDT)[1,2] and the boron neutron capture therapy (BNCT)[3,4] of tumors depends on their efficient translocation across cellular membranes and delivery into specific organelles within cancer cells. For example, the amount of boron-10 needed for effective BNCT treatment has been estimated to be between 15 and 30 $\mu$g/g tumor, depending on the exact location of the boron atoms; 2−5 times less boron is required when it localizes preferentially near the cell nucleus rather than on the plasma membrane.[5,6] Several strategies have been developed to improve the selective delivery of porphyrin sensitizers to tumor tissues, including their conjugation to carrier proteins,[7−9] oligonucleotides,[10,11] monoclonal antibodies,[12−14] epidermal growth factors,[15,16] carbohydrates,[17,18] and hydrophilic polymers (such as HPMA, PVA, PEG, dextran, and poly-lysine).[19,20] The efficient delivery of such conjugates to cancer cells and their subcellular distribution does not only depend on cellular processes, such as transport across the plasma membrane, movement through the cytoplasm, and transport across organelle membranes, but also on the physicochemical properties and structural characteristics that these compounds exhibit.[21−24] Although enhanced cellular uptake and selectivity for tumor tissues have been achieved with some porphyrin sensitizers, most of these are usually found in cytoplasmic membranes rather than in sensitive intracellular sites, such as the mitochondria, the endoplasmic reticulum (ER), and the nuclei. One strategy currently used for drug delivery to these intracellular sites is based on the natural ability of certain proteins and peptide sequences for crossing cell membranes and specifically targeting these organelles. In particular, the role of nuclear localization sequences (NLS) for protein import into the cell nucleus is well documented.[25−28] Generally, an NLS contains a cluster of at least four cationic amino acids (lysine and/or arginine), often flanked by proline or glycine. Among these, the NLS of the simian virus (SV40) large T antigen, P−K−K−K−R−K−V, has been extensively studied.[28] The conjugation of proteins containing the NLS SV40 to chlorin-e6 has been shown to significantly increase the photosensitizing activity of chlor-

in e6.[29] Similarly, the efficient cellular uptake and DNA cleavage ability of a smaller-sized Mn(III)porphyrin−peptide conjugate containing an encoded NLS have been reported.[30] Furthermore, peptide-based shuttles containing multiple NLS SV40 sequences have been conjugated to chlorin-e6 and shown to induce increased photosensitizing activity as a consequence of nuclear delivery, compared with unconjugated chlorin-e6.[31] However, these high molecular weight branched peptide conjugates are difficult to synthesize, purify, and characterize. We have recently reported the efficient conjugation of a porphyrin to several cationic amino acid sequences bearing 1−4 residues and have shown that these conjugates do not localize within cell nuclei, probably due to their short sequences and linkages to the porphyrin ring.[32] Herein we report the synthesis, cellular uptake, phototoxicity, and subcellular localization of two new porphyrin−NLS SV40 conjugates bearing low molecular weight poly-(ethylene glycol) (PEG) linkages.

Another useful approach for cellular delivery of macromolecules involves their conjugation to fusogenic or cell-penetrating peptides, which are normally found in the protein transduction domains responsible for rapid and efficient cellular internalization.[33] Such peptides, including the *Drosophilia* homeotic transcription protein antennapedia (Antp),[34] the human immunodeficiency virus I transcriptional activator (HIV-TAT),[35] and the herpes-virus derived VP22,[36] are potential highly efficient delivery systems for porphyrin sensitizers. Other polypeptides containing 6−15 contiguous arginine residues have been shown to enhance the cellular uptake of several macromolecules.[37,38] However, to date this approach has not yet been used to improve the biological efficacy of porphyrin sensitizers. We report herein the synthesis, cellular uptake, phototoxicity, and subcellular distribution of three new porphyrin conjugates to the membrane translocation peptide HIV-1Tat 48−60 and an octamer of arginine, and we compare them to the two porphyrin−NLS SV40 conjugates also synthesized and evaluated in this study. All conjugates contain PEG-based linkages between the peptides and the porphyrin moieties in order to increase their water solubility and to minimize intramolecular interactions and aggregation in aqueous media.

## Experimental Section

**1. Chemistry.** Unless otherwise indicated, all commercially available starting materials were used directly without further

---

* To whom correspondence should be addressed. Phone: 225-578-7405. Fax: 225-578-3458. E-mail: vicente@lsu.edu.

purification. Reactions under anhydrous conditions were performed in dried and distilled solvents under an argon atmosphere. All reactions were monitored by TLC using Sorbent Technologies 0.25 mm silica gel plates with or without UV indicator (60F-254). Silica gel Sorbent Technologies 32−63 $\mu$m was used for flash column chromatography. $^{1}$H and $^{13}$C NMR were obtained on either a DPX-250 or a ARX-300 Bruker spectrometer. Chemical shifts ($\delta$) are given in ppm relative to CDCl$_3$ (7.26 ppm, $^{1}$H; 77.00 ppm, $^{13}$C) unless otherwise indicated. Electronic absorption spectra were measured on a Perkin-Elmer Lambda 35 UV−vis spectrophotometer. Mass spectra were obtained on an Applied Biosystems QSTAR XL, a hybrid QqTOF mass spectrometer with a MALDI ionization source using CCA as the matrix. CD spectra were obtained in a AVIV Model 202. HPLC separation and analysis were carried out on a Dionex system including a P680 pump and a UVD340U detector. Semipreparative HPLC was carried out using a Luna C$_{18}$ 100 Å, 5 $\mu$m, 10 × 250 mm (Phenomenex, U.S.A.) column and a stepwise gradient; analytical HPLC was carried out using a Delta Pak C$_{18}$ 300 Å, 5 $\mu$m, 3.9 × 150 mm (Waters, U.S.A.) column and a stepwise gradient (deprotected conjugates) or under isocratic conditions (protected conjugates).

**Porphyrin 2.** To a solution of aminoporphyrin **1** (0.200 g, 0.317 mmol) in DMF (1 mL) was added di-glycolic anhydride (0.055 g, 0.476 mmol), and the final solution was stirred at room temperature overnight. The reaction mixture was diluted with 10 mL of CHCl$_3$, followed by hexanes until precipitation occurred. The precipitate was filtered and washed with water to remove residual anhydride and then dried under vacuum to yield 0.237 g (100%) of porphyrin **2**. HPLC (solvent system 1): $t_r$ = 4.24 min. UV−vis (CHCl$_3$) $\lambda_{max}$ ($\epsilon$/M$^{-1}$ cm$^{-1}$): 414 (406 000), 512 (16 900), 547 (9000), 589 (5400), 645 (4100). $^{1}$H-NMR ($d_6$-DMSO, 300 MHz): $\delta$ 10.39 (1H, s), 8.82−8.90 (8H, m), 8.10−8.31 (10H, m), 7.82−7.84 (9, m), 4.36 (2H, s), 4.34 (2H, s), −2.91 (2H, s). $^{13}$C-NMR (CDCl$_3$, 75 MHz): 171.93, 168.38, 156.13, 141.22, 138.42, 136.28, 134.69, 134.22, 131.41, 131.01, 128.09, 127.10, 119.99, 117.94, 70.69, 68.30. HRMS (MALDI) $m/z$ 746.2799 (M + H$^+$), calculated for C$_{48}$H$_{35}$N$_5$O$_4$ 746.2689.

**Porphyrin 3.** To a solution of porphyrin **2** (0.100 g, 0.134 mmol) in DMF (1 mL) were added DIEA (0.104 g, 0.804 mmol), HOBt (0.020 g, 0.134 mmol), and TBTU (0.042 g, 0.134 mmol). After the mixture was stirred for 5 min, NH$_2$CH$_2$CH$_2$(OCH$_2$CH$_2$)$_5$OCH$_2$CO$_2$$^t$Bu (0.053 g, 0.134 mmol) was added, and stirring continued for 48 h at room temperature. The reaction mixture was diluted with 50 mL of ethyl acetate, washed with water (3 × 100 mL), and dried over anhydrous Na$_2$SO$_4$, and the solvent was evaporated under vacuum. The target porphyrin was purified by flash chromatography on silica gel using ethyl acetate followed by ethyl acetate:methanol 90:10 for elution, yielding 0.193 g (64%) of the *tert*-butyl ester of porphyrin **3**. HPLC (solvent system 5): $t_r$ = 7.53 min. UV−vis (CHCl$_3$) $\lambda_{max}$ ($\epsilon$/ M$^{-1}$ cm$^{-1}$): 419 (452 700), 516 (17 400), 551 (8800), 590 (5600), 646 (4300). $^{1}$H-NMR (CDCl$_3$, 300 MHz): $\delta$ 8.89−8.95 (5H, m), 8.24−8.26 (6H, m), 8.15 (2H, d, $J$ = 8.16 Hz), 7.77−7.78 (9H, m), 7.61 (1H, s), 4.42 (2H, s), 4.33 (2H, s), 4.02 (2H, s), 3.66−3.68 (24H, m), 1.48 (9H, s), −2.70 (2H, s). $^{13}$C-NMR (CDCl$_3$, 75 MHz): $\delta$ 169.64, 169.29, 167.83, 142.08, 138.08, 137.42, 135.02, 134.49, 131.12, 127.67, 126.64, 120.01, 119.65, 118.42, 81.59, 71.91, 71.46, 70.53, 70.33, 70.07, 69.67, 68.85, 38.99, 28.04. HRMS (MALDI) $m/z$ (M + H$^+$) 1123.5199, calculated for C$_{66}$H$_{70}$N$_6$O$_{11}$ 1122.5103. To a solution of the *tert*-butyl protected porphyrin **3** (0.068 g, 0.061 mmol) in 1 mL of dichloromethane was added 1 mL of TFA, and the final mixture was stirred at room temperature for 4 h. After removal of the solvent under vacuum, the residue was triturated and washed with Et$_2$O to afford porphyrin **3** as a green solid in quantitative yield (0.065 g). HPLC (solvent system 1): $t_r$ = 17.05 min. UV−vis (CHCl$_3$) $\lambda_{max}$ ($\epsilon$/M$^{-1}$ cm$^{-1}$): 421 (354 400), 513 (15 000), 549 (7200), 589 (4500), 645 (3300). $^{1}$H-NMR (CDCl$_3$, 300 MHz): $\delta$ 8.72−8.74 (8H, m), 8.61−8.63 (8H, m), 8.37 (2H, d, $J$ = 8.28 Hz), 7.98−8.07 (10H, m), 4.48 (2H, s), 4.41 (2H, s), 4.17 (2H, s), 3.68−3.72 (24H, m), −0.68 (2H, s). $^{13}$C NMR (CDCl$_3$, 75 MHz): $\delta$ 173.49, 171.18, 169.31, 139.36, 139.15, 138.29, 136.21, 130.37,

128.87, 128.71, 128.46, 119.09, 116.09, 112.28, 71.15, 70.57, 70.10, 70.03, 69.92, 69.80, 39.29. HRMS (MALDI) $m/z$ (M + H$^+$) 1067.4586, calculated for C$_{62}$H$_{63}$N$_6$O$_{11}$ 1067.4554.

**Porphyrin 8.** Under an argon atmosphere, porphyrin **7** (0.400 g, 0.589 mmol) was dissolved in 15 mL of anhydrous DMSO. To this solution was added Cs$_2$CO$_3$ (0.384 g, 1.178 mmol), and the mixture was heated to 50 °C for 1 h. Benzylbromo acetate (0.269 g, 1.178 mmol) was added in one portion, and the final mixture was heated at 60 °C for 2 h. The reaction mixture was cooled to room temperature and diluted with 100 mL of ethyl acetate. The organic phase was washed with water (3 × 100 mL) and dried over anhydrous Na$_2$SO$_4$, and the solvent evaporated under vacuum. Porphyrin **8** was purified by flash chromatography on silica gel using chloroform/methanol 95:5 for elution, and it was isolated in 30% yield (0.145 g). HPLC (solvent system 1): $t_r$ = 5.90 min. UV−vis (CHCl$_3$) $\lambda_{max}$ ($\epsilon$/M$^{-1}$ cm$^{-1}$) 421 (363 900), 520 (32 200), 557 (23 900), 594 (12 200), 651 (10 500). $^{1}$H NMR ($d_6$-acetone, 300 MHz): $\delta$ 8.85−8.92 (10H, m), 8.01−8.15 (8H, m), 7.28−7.65 (15H, m), 5.36 (2H, s), 5.11 (2H, s), −2.75 (2H, s). $^{13}$C NMR ($d_6$-acetone, 75 MHz): $\delta$ 169.64, 159.15, 158.50, 150.36, 147.86, 143.32, 136.54, 136.34, 136.07, 134.09, 129.48, 129.20, 121.16, 120.31, 114.77, 114.00, 67.34, 66.21. HRMS (MALDI) $m/z$ (M + H$^+$) 827.2838, calculated for C$_{53}$H$_{38}$N$_4$O$_6$ 827.2869.

**Porphyrin 9.** Under an argon atmosphere porphyrin **8** (0.110 g, 0.133 mmol) was dissolved in 12 mL of phenol-free acetone, and K$_2$CO$_3$ (0.110 g, 0.798 mmol) was added to the solution. The reaction mixture was refluxed for 1 h, and then *tert*-butylbromo acetate (0.156 g, 0.798 mmol) was added in one portion. The final mixture was refluxed overnight. After removal of the solvent under vacuum, the purple residue was dissolved in ethyl acetate (100 mL), washed with water (2 × 50 mL), and dried over anhydrous Na$_2$SO$_4$, and the solvent evaporated under vacuum. The target porphyrin was purified by flash chromatography on silica gel using chloroform for elution and isolated in 93% yield (0.145 g). HPLC (solvent system 6): $t_r$ = 6.01 min. UV−vis (CHCl$_3$) $\lambda_{max}$ ($\epsilon$/M$^{-1}$ cm$^{-1}$) 422 (394 000), 517 (17 260), 553 (11 100), 591 (6300), 647 (7300). $^{1}$H NMR (CDCl$_3$, 300 MHz): $\delta$ 8.90−8.93 (8H, m), 8.07−8.19 (8H, m), 7.24−7.53 (15H, m), 5.43 (2H, s), 5.01 (2H, s), 4.88 (6H, s), −2.68 (2H, s). $^{13}$C NMR (CDCl$_3$, 75 MHz): $\delta$ 168.53, 168.15, 157.80, 150.30, 145.93, 144.82, 135.51, 135.38, 128.67, 128.53, 119.55, 112.89, 82.56, 67.16, 66.02, 65.54, 28.14. HRMS (MALDI) $m/z$ (M + H$^+$) 1169.4928, calculated for C$_{71}$H$_{68}$N$_4$O$_{12}$ 1169.4912. The benzyl protected porphyrin **9** (0.120 g, 0.102 mmol) was dissolved in 4 mL of a mixture of glacial acetic acid/ethanol 3:1. The solution was flushed with H$_2$, and then 10% Pd/C (0.120 mg) was added. The reaction mixture was flushed once again with H$_2$, capped with a H$_2$-filled balloon, and stirred at room temperature for 4 h. The reaction mixture was filtered through Celite to remove the catalyst, and the solid residue was washed with chloroform/methanol 2:1. The filtrate was evaporated under vacuum, and the residue was dissolved in chloroform (50 mL) and washed with water (3 × 50 mL) to remove traces of acid. The organic phase was dried over anhydrous Na$_2$SO$_4$, and the solvent evaporated under vacuum. Porphyrin **9** was purified by flash chromatography on silica gel using chloroform/methanol 9:1 for elution and isolated in 83% yield (0.092 g). HPLC (solvent system 7): $t_r$ = 15.27 min. UV−vis (acetone) $\lambda_{max}$ ($\epsilon$/M$^{-1}$ cm$^{-1}$) 422 (350 400), 517 (36 300), 553 (15 300), 591 (6800), 647 (7200). $^{1}$H NMR ($d_6$-acetone, 300 MHz): $\delta$ 8.87 (8H, s), 8.13−8.15 (8H, m), 7.38−7.41 (10H, m), 5.03 (2H, s), 4.91 (6H, s), 1.58 (27H, s), −2.73 (2H, s). $^{13}$C NMR ($d_6$-acetone, 75 MHz): $\delta$ 172.81, 172.53, 159.62, 136.28, 135.74, 120.64, 118.61, 114.08, 82.39, 66.59, 28.38. HRMS (MALDI) $m/z$ (M + H$^+$) 1079.4454, calculated for C$_{64}$H$_{62}$N$_4$O$_{12}$ 1079.4442.

**Peptide Synthesis.** Peptide sequences were prepared on an automated peptide synthesizer (Applied Biosystems Pioneer, Peptide Synthesis System, U.S.A.) in a 0.2 mmol scale, using the Fmoc strategy of solid-phase peptide synthesis. A 4-fold excess of the Fmoc protected amino acids were coupled to the PAL-PEG-PS resin using TBTU/HOBt or HATU/HOBt as the activating agents. The peptide sequences prepared using this methodology were as follows: GPKKKRKVNH$_2$, GRRRRRRRRCOOH, and GRKKR-

RQRRRPPQNH$_2$. After the final coupling and the successive removal of the Fmoc group, the resin was washed with DMF and isopropyl alcohol and then dried under vacuum. The dried resin containing the protected amino acid sequences were used in the coupling reaction to the porphyrin derivatives (vide infra).

**Pegylation of Peptides.** Peptidyl resin (0.025 mmol) was introduced into a glass synthesizer, swelled in DMF for 1 h, and then washed with DMF (2 × 5 mL). To the resin was added 500 $\mu$L of a solution containing 0.05 mmol of FmocNH(CH$_2$CH$_2$O)$_7$-CH$_2$CH$_2$NHCOCH$_2$OCH$_2$CO$_2$H, 0.150 mmol of DIEA, 0.05 mmol of HOBt, and 0.05 mmol of TBTU. The reaction mixture was allowed to react until the Kaiser test was negative, and then the resin was washed with DMF (5 × 5 mL) to remove residual reactants. The Fmoc protecting group was removed by treatment with 20% piperidine/DMF for 40 min at room temperature, washed with DMF (5 × 5 mL), dichloromethane (3 × 5 mL), and methanol (3 × 5 mL), and then dried under vacuum. The dried resin containing the peglyted protected amino acid sequences were used in the coupling reaction to the porphyrin derivatives (vide infra).

**General Procedure for Syntheses of Porphyrin Conjugates.** Peptidyl resin (0.025 mmol) was introduced into a glass synthesizer, swelled in DMF for 1 h, and then washed with DMF (2 × 5 mL). To the peptidyl resin was added 500 $\mu$L of a solution containing 0.05 mmol of porphyrin **3** or **9**, 0.150 mmol of DIEA, 0.05 mmol of HOBt, and 0.05 mmol of TBTU. The reaction mixture was shaken overnight at room temperature and then filtered to give a dark purple resin. The resin was washed to remove unreacted porphyrin, first with DMF until the filtrate was colorless and then with dichloromethane and methanol, before being dried under vacuum. Cleavage and deprotection was carried out by treatment of the dried resin with 3 mL of a mixture of TFA/phenol/TIS/H$_2$O, 88/5/2/5, at room temperature for 4 h. The resin was filtered and washed with TFA (3 × 2 mL), and the filtrates were combined and evaporated under vacuum to give a green residue. Addition of cold Et$_2$O yielded a green precipitate, which was washed repeatedly with Et$_2$O and dried under vacuum. The purification of the porphyrin conjugates was achieved by reverse phase HPLC on a Luna C$_{18}$ semipreparative column (10 × 250 mm, 5 $\mu$m) (Phenomenex, U.S.A.) using a buffer system of water/acetonitrile both containing 0.1% TFA, with a stepwise gradient from 60 to 95%. The fraction containing the conjugate was collected and lyophilized to yield pure conjugate. The purity of the peptides was >98% as obtained by HPLC on an analytical Delta Pak C$_{18}$ (3.9 × 150 mm, 5 $\mu$m) column.

**Conjugate 4:** 0.026 g, 52% yield. HPLC: solvent system 1, $t_r$ = 6.97 min; solvent system 2, $t_r$ = 16.87 min. UV−vis (methanol) $\lambda_{max}$ ($\epsilon$/M$^{-1}$ cm$^{-1}$) 415 (239 700), 512 (10 900), 548 (7800), 589 (4700), 645 (3600). $^1$H NMR (D$_2$O, 300 MHz): $\delta$ 8.70 (2H, d, $J$ = 17.98 Hz), 8.28 (2H, d, $J$ = 6.29 Hz), 8.1 (1H, s), 4.41−4.51 (6H, m), 4.28 (4H, s), 3.60−3.77 (24H, m), 2.97−3.01 (8H, m), 1.29−2.09 (32H, m), 0.93 (6H, s). HRMS (MALDI) $m/z$ (M + H$^+$), 1988.1018, calculated for C$_{104}$H$_{142}$N$_{22}$O$_{18}$ 1988.0872.

**Conjugate 5:** 0.028 g, 47% yield. HPLC: solvent system 1, $t_r$ = 6.73 min; solvent system 2, $t_r$ = 14.55 min. UV−vis (methanol) $\lambda_{max}$ ($\epsilon$/M$^{-1}$ cm$^{-1}$) 422 (220 400), 512 (10 500), 547 (5200), 588 (3100), 645 (2400). $^1$H NMR (D$_2$O, 300 MHz): $\delta$ 8.66 (2H, s), 8.25 (2H, d, $J$ = 9.31 Hz), 8.12 (7H, s), 4.41 (1H, s), 4.29−4.31 (5H, m), 4.08 (2H, s), 3.96 (2H, s), 3.67−3.77 (22H, m), 3.60−3.61 (2H, m), 3.16−3.21 (16H, m), 1.63−1.78 (32H, m). HRMS (MALDI) $m/z$ (M + H$^+$) 2373.2799, calculated for C$_{112}$H$_{161}$N$_{39}$O$_{20}$ 2373.2780

**Conjugate 6:** 0.032 g, 46% yield. HPLC: solvent system 1, $t_r$ = 6.42 min; solvent system 2, $t_r$ = 14.43 min. UV−vis (methanol) $\lambda_{max}$ ($\epsilon$/M$^{-1}$ cm$^{-1}$) 422 (249 000), 512 (12 100), 547 (5900), 588 (3600), 645 (2700). $^1$H NMR (D$_2$O, 300 MHz): $\delta$ 8.90 (6H, s), 8.61 (6H, s), 8.19 (2H, d, $J$ = 7.47 Hz), 8.04 (6H, s), 4.25−4.39 (13H, m), 4.08 (3H, s), 3.96 (3H, s), 3.58−3.75 (39H, m), 3.17−3.19 (21H, m), 2.96−3.01 (8H, t, $J$ = 8.5 Hz), 2.32−2.40 (10H, m), 1.25−2.02 (76H, m). HRMS (MALDI) $m/z$ (M + H$^+$) 2766.4987, calculated for C$_{132}$H$_{193}$N$_{42}$O$_{25}$ 2766.5044.

**Conjugate 10:** 0.008 g, 14% yield. HPLC: solvent system 4, $t_r$ = 5.09 min; solvent system 3, $t_r$ = 8.45 min. UV−vis (methanol) $\lambda_{max}$ ($\epsilon$/M$^{-1}$ cm$^{-1}$) 418 (227 200), 516 (4600), 553 (3700), 591 (2400), 649 (2200). $^1$H NMR (D$_2$O, 300 MHz): $\delta$ 7.95 (2H, d, $J$ = 9.32 Hz), 7.39−7.47 (6H, m), 7.16 (1H, d, $J$ = 9.13 Hz), 6.83 (1H, d, $J$ = 10.13 Hz), 4.26−4.28 (4H, m), 4.01−4.10 (6H, m), 3.46−3.71 (34H, m), 3.17−3.21 (4H, s), 2.96−3.01 (8H, m), 1.13−2.00 (32H, m), 0.98 (6H, s). HRMS (MALDI) $m/z$ (M + H$^+$) 2299.1524, calculated for C$_{114}$H$_{157}$N$_{22}$O$_{29}$ 2299.1517.

**Conjugate 11:** 0.010 g, 13% yield. HPLC: solvent system 4, $t_r$ = 5.63 min, solvent system 3, $t_r$ = 6.15 min. UV−vis (methanol) $\lambda_{max}$ ($\epsilon$/M$^{-1}$ cm$^{-1}$) 422 (225 600), 517 (5500), 554 (4400), 592 (2700), 650 (2600). $^1$H NMR (D$_2$O, 300 MHz): $\delta$ 7.86−7.93 (2H, m), 7.69−7.77 (2H, m), 7.48−7.53 (2H, m), 4.32 (6H, s), 4.20 (2H, s), 4.03 (2H, s), 3.66−3.71 (32H. m), 3.38−3.48 (2H, m), 3.20 (8H, s), 2.97−3.03 (2H, m), 1.28−2.51 (32H, m). HRMS (MALDI) $m/z$ (M + H$^+$) 3077.5678, calculated for C$_{142}$H$_{207}$N$_{42}$O$_{36}$ 3077.5687.
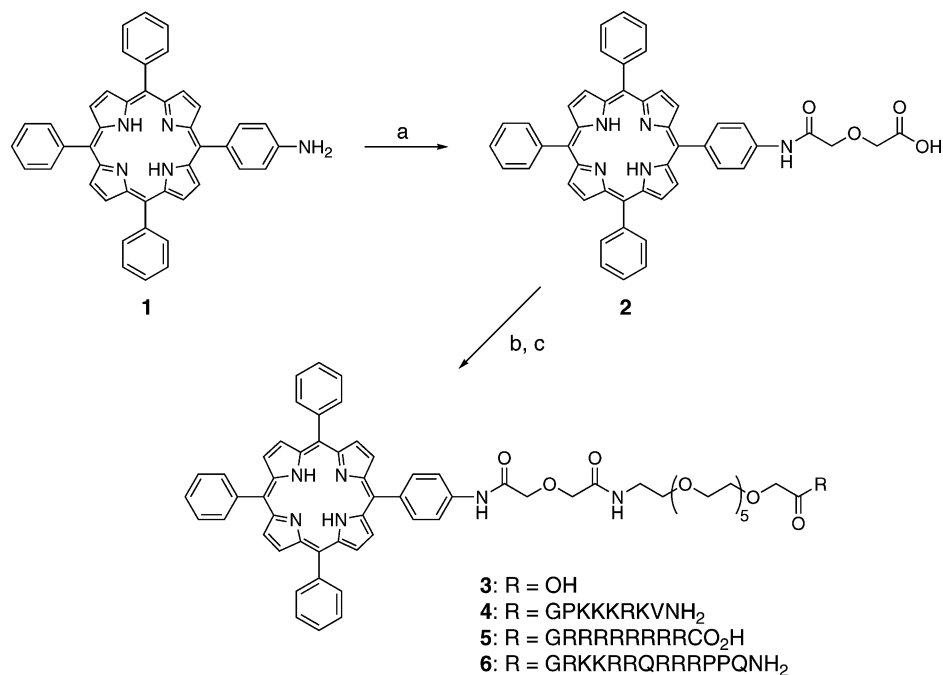
**2. Cell Culture.** All tissue culture media and reagents were obtained from Invitrogen. Human HEp2 cells were obtained from ATCC and maintained in a 50:50 mixture of DMEM:Advanced MEM containing 5% FBS. The cells were subcultured biweekly to maintain subconfluent stocks.

**2.1. Time-Dependent Cellular uptake.** HEp2 cells were plated at 10 000 per well in a Costar 96-well plate and allowed to grow overnight. Conjugate stocks were prepared in water at a concentration of 10 mM and then diluted into medium to final working concentrations. The cells were exposed to 10 $\mu$M of each conjugate for 0, 1, 2, 4, 8, and 24 h. At the end of the incubation time the loading medium was removed, and the cells were washed with PBS. The cells were solubilized upon addition of 100 $\mu$L of 0.25% Triton X-100 (Calbiochem) in PBS. To determine the conjugate concentration, fluorescence emission was read at 410/650 nm (excitation/ emission) using a BMG FLUOstar plate reader. The cell numbers were quantified using the CyQuant reagent (Molecular Probes).

**2.2. Dark Cytotoxicity.** The HEp2 cells were plated as described above and allowed 36−48 h to attach. The cells were exposed to increasing concentrations of conjugate up to 100 $\mu$M and incubated overnight. The loading medium was then removed, and the cells were fed medium containing Cell Titer Blue (Promega) as per manufacturer's instructions. Cytotoxicity was then measured by reading the fluorescence at 520/584 nm using a BMG FLUOstar plate reader. The signal was normalized to 100% viable (untreated) cells and 0% viable (treated with 0.2% saponin from Sigma) cells.

**2.3. Phototoxicity.** The HEp2 cells were prepared as described above for the dark cytotoxicity assay and treated with conjugate concentrations of 0, 0.625, 1.25, 2.5, 5, and 10 $\mu$M. After compound loading, the medium was removed and replaced with medium containing 50 mM HEPES pH 7.4. The cells were then placed on ice and exposed to light from a 100 W halogen lamp filtered through a 610 nm long pass filter (Chroma) for 10 min. An inverted plate lid filled with water to a depth of 5 mm acted as an IR filter. The total light dose was approximately 0.5 J/cm$^2$. The cells were returned to the incubator overnight, and the cytotoxicity was assayed as described above.

**2.4. Intracellular Localization.** The HEp2 cells were plated on LabTek 2 chamber coverslips and incubated overnight, before being exposed to 10 $\mu$M of conjugate for either 2 or 18 h. For the co-localization experiments, the cells were incubated for 18 h concurrently with conjugate and one of the following organelle tracers, for 30 min: 250 nM MitoTracker Green (Molecular Probes), 50 nM LysoSensor Green (Molecular Probes), and 5 $\mu$g/mL DiOC$_6$ (Molecular Probes). The slides were washed three times with growth medium, and new medium containing 50 mM HEPES pH 7.4 was added. Fluorescent microscopy was performed using a Zeiss Labovert 200M inverted fluorescence microscope fitted with standard FITC and Texas Red filter sets (Chroma). The images were aquired with a Zeiss Axiocam MRM CCD camera fitted to the microscope.

**Scheme 1**[a]



**3**: R = OH
**4**: R = GPKKKRKVNH$_2$
**5**: R = GRRRRRRRRCO$_2$H
**6**: R = GRKKRRQRRRPPQNH$_2$

[a] Reactions and conditions: (a) diglycolic anhydride, DMF, rt, 24 h (100%); (b) HOBt/TBTU/DIEA, NH$_2$CH$_2$CH$_2$(OCH$_2$CH$_2$)$_5$OCH$_2$CO$_2$$^t$Bu, rt, 48 h (64%), then TFA, rt, 4 h (100%); (c) HOBt/TBTU/DIEA, peptidyl resin, rt, 24 h, then TFA/H$_2$O/phenol/TIS, 88/5/5/2, rt, 4 h (46−52%).
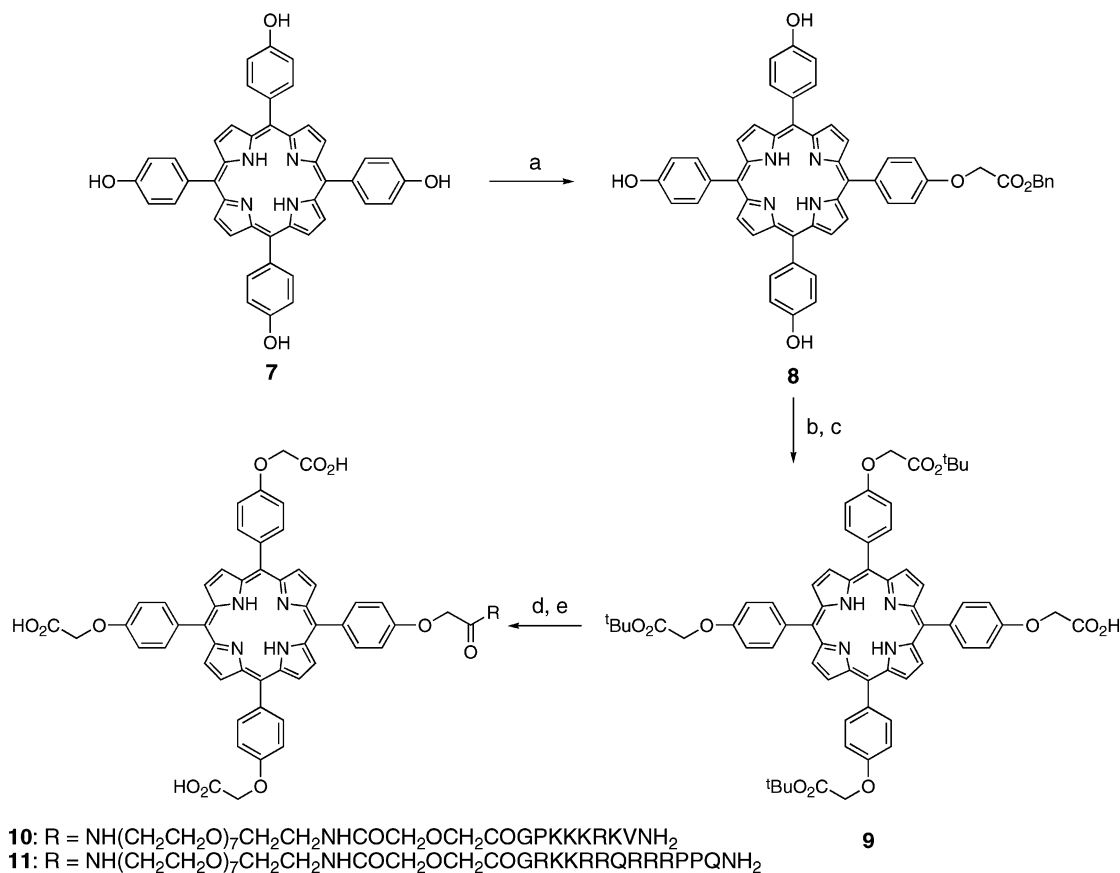
## Results and Discussion

**1. Synthesis and Characterization.** Porphyrin conjugates **4**, **5**, **6**, **10**, and **11** were designed to contain a peptide sequence (NLS or fusogenic peptide) linked by a low molecular weight PEG in order to minimize intramolecular interactions between the porphyrin and the peptide moieties and to enhance their water solubility. Previous studies have shown that PEG−drug conjugates display enhanced water solubility, serum life, and tumor accumulation.[39] The synthesis of high molecular weight PEG−porphyrin conjugates has been reported by several groups; however, complex mixtures are often obtained due to the PEG's polydispersity.[40,41] Furthermore, high molecular weight conjugates might have decreased ability for crossing cellular membranes and other biological barriers. We recently showed, using molecular modeling calculations (using the Gasteiger-Huckel model and the Tripos Force Field parameters incorporated into the SYBYL 7.0 software package), that porphyrin−peptide conjugates bearing short (up to five atom) spacers preferentially adopt a bent conformation in order to maximize intramolecular hydrophobic and hydrogen-bond interactions.[32] Similar calculations using various oligomeric PEGs, aminoporphyrin **1**, and peptide G-P-K-K-K-R-K-V (results not shown) indicated that a 20-atom spacer minimized folding of the peptide over the porphyrin ring, thus favoring an extended vs bent structure for the conjugates. Such an extended structure should allow the peptide to adopt a favorable conformation for binding to import receptors.[42] We therefore chose to use the two protected heterofunctional PEGs FmocNH(CH$_2$CH$_2$O)$_7$CH$_2$CH$_2$NHCOCH$_2$-OCH$_2$CO$_2$H and $^t$BuO$_2$CCH$_2$O(CH$_2$CH$_2$O)$_5$CH$_2$CH$_2$NH$_2$ in the synthesis of our conjugates. While the first compound is commercially available, the latter was prepared in 33% overall yield from hexaethylene glycol, as described in the literature (see Supporting Information).[43] Two series of conjugates were synthesized bearing either an hydrophobic porphyrin (**4**, **5**, and **6**) or an hydrophilic one (**10** and **11**) in order to evaluate the effect of this structural parameter on the cellular uptake, phototoxicity, and intracellular localization of the porphyrin−peptide conjugates.

Conjugates **4**, **5**, and **6** were synthesized as shown in Scheme 1 from mono-aminoporphyrin **1**, which is easily prepared on a multigram scale from *meso*-tetraphenylporphyrin and displays high solubility in organic solvents.[44] The conversion of the amino group of porphyrin **1** to the carboxylic acid **2** was achieved quantitatively by reaction with diglycolic anhydride in DMF. The coupling of porphyrin **2** with *tert*-butyl protected PEG in solution phase, followed by deprotection using TFA, gave the free carboxylic acid porphyrin **3** in 64% overall yield. This porphyrin, as the hydroxybenzotriazole (HOBt) ester, was coupled to the peptidyl-PAL-PEG-PS resin, and following cleavage and deprotection from the solid support with TFA/phenol/TIS/H$_2$O, 88/5/2/5, the water soluble conjugates **4**−**6** were isolated in 46−52% yield.

The carboxylic acid functionalized conjugates **10** and **11** were synthesized from commercially available porphyrin **7** as shown in Scheme 2. The initial protection of one hydroxyl group of **7** was accomplished by Williamson alkylation using benzyl bromoacetate; although a mixture of all possible substituted ethers was obtained, careful optimization of the reaction conditions (ratio of reagents **7**/Cs$_2$CO$_3$/benzyl bromoacetate 1/2/2, and 2 h reaction time at 60 °C) afforded the mono-ether **8** in 30% yield. The remaining hydroxyl groups were alkylated using *tert*-butyl bromoacetate in 93% yield, and subsequent removal of the benzyl group by catalytic hydrogenation gave carboxylic acid porphyrin **9** in 83% yield. The coupling of **9** to the peptidyl-PAL-PEG-PS resin was performed as described above. After cleavage and deprotection from the solid support, the free carboxylic acid conjugates **10** and **11** were isolated by reverse phase HPLC in 13−14% yield. The lower yields obtained in this case may be caused by steric effects resulting from the close proximity of the porphyrin ring to the carboxylic group during the coupling reaction and by the likely formation of aggregates in the solvent used.

All conjugates were purified by reverse phase HPLC and characterized by HRMS, UV−vis, and $^1$H NMR. Although the NMR chemical shifts of the Cα peptidyl protons can be useful in the assignment of peptide secondary structures, we were not

**Scheme 2**[a]



**10**: R = NH(CH₂CH₂O)₇CH₂CH₂NHCOCH₂OCH₂COGPKKKRKVNH₂
**11**: R = NH(CH₂CH₂O)₇CH₂CH₂NHCOCH₂OCH₂COGRKKRRQRRRPPQNH₂

[a] Reactions and conditions: (a) $Cs_2CO_3$, $BrCH_2CO_2Bn$, DMSO, 60 °C, 2 h (30%); (b) $K_2CO_3$, $BrCH_2CO_2^tBu$, acetone reflux, 4 h (93%); (c) 10% Pd/C, glacial $CH_3CO_2H$/ethanol, rt, 4 h (83%); (d) HOBt/TBTU/DIEA, $NH_2$-PEG-peptidyl-PAL-PEG-PS resin, rt, 48 h; (e) TFA/$H_2O$/phenol/TIS, 88/5/5/2, rt, 4 h (13−14%).

able to use this technique due to overlap of these signals with the solvent. Circular dichroism (CD) is another important technique for the determination of the secondary structures of peptides and other molecules in solution.[45] The CD spectra of porphyrin conjugates **4**, **5**, and **6** in buffer solution (10 mM TRIS, pH 7.5, with 20% TFE (v/v)) and in 10 mM TRIS buffered water were determined (see Figure S1 of the Supporting Information). In the amide region (190−250 nm), these porphyrin conjugates show negative Cotton effects at around 200 nm (**4**, $[\Phi]_{MRW} = -10\ 530$ deg cm² dmol⁻¹ at 199 nm; **5**, $[\Phi]_{MRW} = -15\ 190$ deg cm² dmol⁻¹ at 198 nm; **6**, $[\Phi]_{MRW} = -133\ 600$ deg cm² dmol⁻¹ at 199 nm). These CD spectra indicate that the peptides in these conjugates adopt a random coil structure under the conditions used (the CD spectrum of the random coil peptide is, for instance, $[\Phi]_{MRW} = -41\ 900$ deg cm² dmol⁻¹ at 197 nm for poly(Lys) at pH 7).[45] Some of the intensity in the 200 nm region (especially for conjugate **6**) may be due to induced CD effects of the *meso*-phenyl groups of the porphyrin, as is observed in phenylalanine-containing peptides.[45] Therefore it is likely that in these conjugates the peptides are not bent over the porphyrin ring. For conjugate **4**, these results are in agreement with the crystal structure reported for the complex kariopherin α/SV40, a protein that binds the nucleoporins involved in nuclear import.[46] For conjugate **6**, the results obtained are in agreement with previous CD data reported for the Tat protein, showing that the highly basic region from 49 to 60 (with the sequence R-K-K-R-R-Q-R-R-R) adopts an extended conformation due to the electrostatic repulsion between the positively charged side chains.[47]
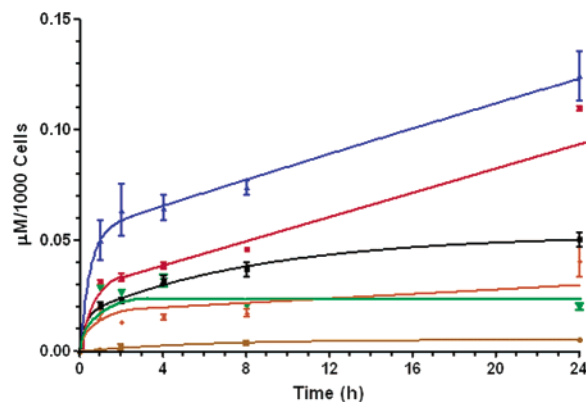


**Figure 1.** Time-dependent uptake of porphyrin **3** (brown) and of conjugates **4** (black), **5** (red), **6** (blue), **10** (green), and **11** (orange) at 10 μM by HEp2 cells.

**2. Cell Culture Studies. 2.1. Time-Dependent Cellular Uptake.** The time-dependent uptake of all conjugates at a concentration of 10 μM in human HEp2 cells was investigated and the results are shown in Figure 1. For comparison purposes, the uptake of unconjugated porphyrin **3** was also determined. The cellular uptake was significantly enhanced for all porphyrin−peptide conjugates compared with **3** and depends on the nature and sequence of the amino acid residues and on the substituents at the porphyrin periphery, i.e., on the overall molecular charge and its distribution. As expected, conjugate **6** bearing the cell-penetrating peptide HIV-1Tat accumulated the most within cells at all time points studied, followed by the octa-arginine conjugate **5**. The SV40 conjugate **4**, also contain-
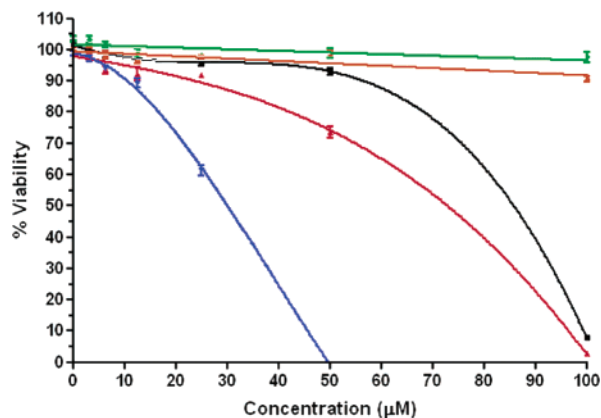
**Figure 2.** Dark toxicity of porphyrin conjugates **4** (black), **5** (red), **6** (blue), **10** (green), and **11** (orange) toward HEp2 cells using the Cell Titer Blue assay.

ing an hydrophobic porphyrin, was the least accumulated within cells of this series, indicating that peptides bearing multiple arginine residues are more efficient in delivering porphyrins into cells. Our results are in agreement with previous studies showing that positively charged guanidinium groups play an important role in facilitating cellular uptake, probably by forming bidentate hydrogen bonds with membrane-containing phosphate groups.[32,37]

All conjugates showed similar uptake kinetics, with a rapid accumulation within cells in the first 1 h, followed by a slower uptake at longer time points. In the case of conjugate **10**, bearing a NLS SV40 sequence, a plateau was reached after 4 h. Interestingly, conjugates **10** and **11**, containing three carboxylic groups at the periphery of the porphyrin ring, were the least taken-up by cells at long time points (>4 h). While the uptake of both conjugates was rapid in the first 1−2 h, a significant difference was observed in the amount accumulated after 24 h, which was clearly higher for the HIV-1 Tat conjugate **11** than for the SV40 conjugate **10**. However, in comparison with **6** bearing the same HIV-1 Tat peptide sequence, conjugate **11** was taken-up to a much lower extent at all time points studied. While at short times (up to 4 h) the SV40 conjugates **4** and **10** showed similar uptake into cells, at longer time points conjugate **4** clearly accumulated to a much higher extent within cells compared with **10**. These results clearly indicate, for the first time, that not only the nature of the peptide sequence but also the structure of the porphyrin ring deeply influence the uptake of these conjugates by cells.

**2.2. Cytotoxicity.** The dark cytotoxicity and phototoxicity of the new porphyrin conjugates were evaluated in human HEp2 cells exposed to increasing concentrations of each conjugate for 18 h, as shown in Figures 2 and 3, respectively. Conjugates **10** and **11**, the least accumulated within cells (vide supra), show no toxicity at concentrations up to 100 $\mu$M in the dark and no phototoxicity upon exposure to low light dose (0.5 J/cm$^2$) up to 10 $\mu$M concentrations. On the other hand, conjugates **4**, **5**, and **6** showed IC$_{50}$ = 90, 75, and 30 $\mu$M in the dark, respectively. These results are in agreement with the cellular uptake studies describe above, which show that the amount of conjugate taken-up by cells increases in the order **4** < **5** < **6** (Figure 1). On the other hand, the most phototoxic compound (IC$_{50}$ = 1.5 $\mu$M) was found to be **4**, bearing an NLS SV40 peptide conjugated to an hydrophobic porphyrin, followed by **5** and **6**, bearing the fusogenic peptides (Figure 3). Since conjugate **4** accumulates to a much lower extent within the cells compared with **5** and **6**, its high phototoxicity could be a result of its preferential localization within more sensitive cell compartments. Our results show, as has been previously
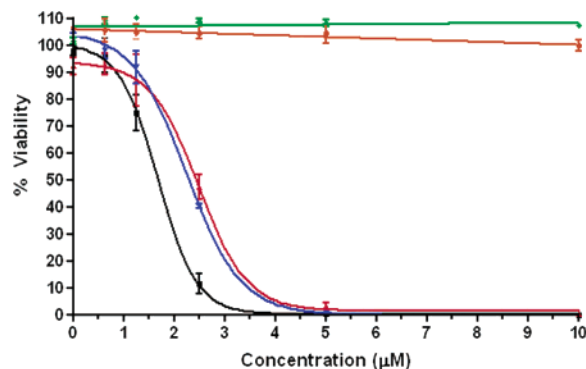


**Figure 3.** Phototoxicity of porphyrin conjugates **4** (black), **5** (red), **6** (blue), **10** (green), and **11** (orange) toward HEp2 cells using 0.5 J/cm$^2$ dose light.
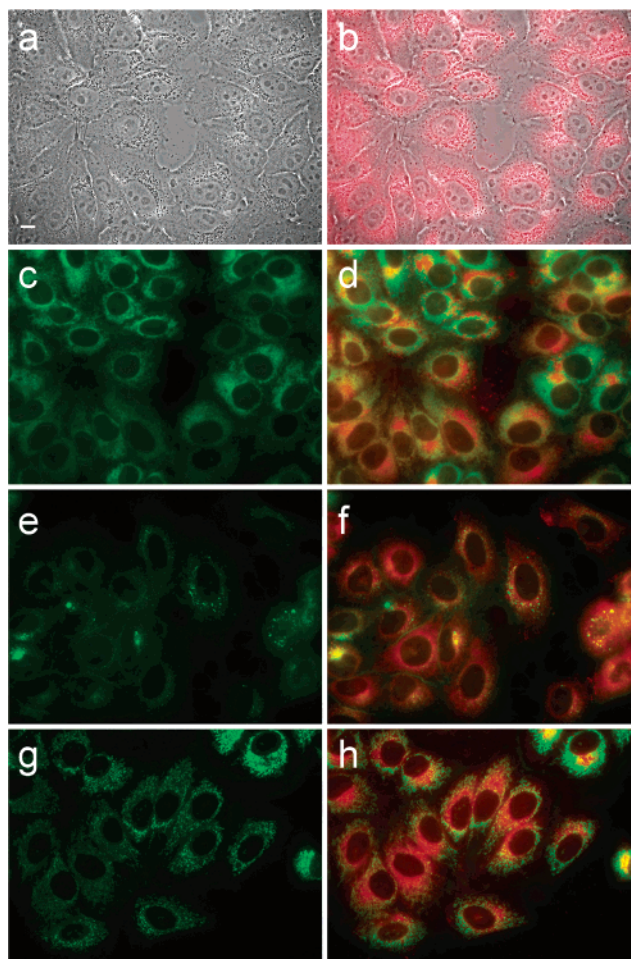


**Figure 4.** Subcellular localization of conjugate **4** in HEp2 cells at 10 $\mu$M for 18 h: (a) phase contrast, (b) overlay of **4** fluorescence and phase contrast, (c) DiOC$_6$ fluorescence, (d) overlay of DiOC$_6$ with **4** fluorescence, (e) LysoSensor Green fluorescence, (f) overlay of LysoSensor Green with **4** fluorescence, (g) MitoTracker Green fluorescence, (h) overlay of MitoTracker Green with **4** fluorescence. Scale bar: 10 $\mu$m.

observed,[24] that not only the amount of sensitizer accumulated within target cells but also its subcellular distribution determine its phototoxicity and, ultimately, its biological efficacy.

**2.3. Intracellular Localization.** The subcellular localization of all conjugates was investigated in HEp2 cells at short (2 h) and long (18 h) time points, using fluorescence microscopy. No differences in the fluorescent patterns were observed at the two time points, although a decrease in signal intensity was evident at the short incubation time. Figures 4 and 5 show the
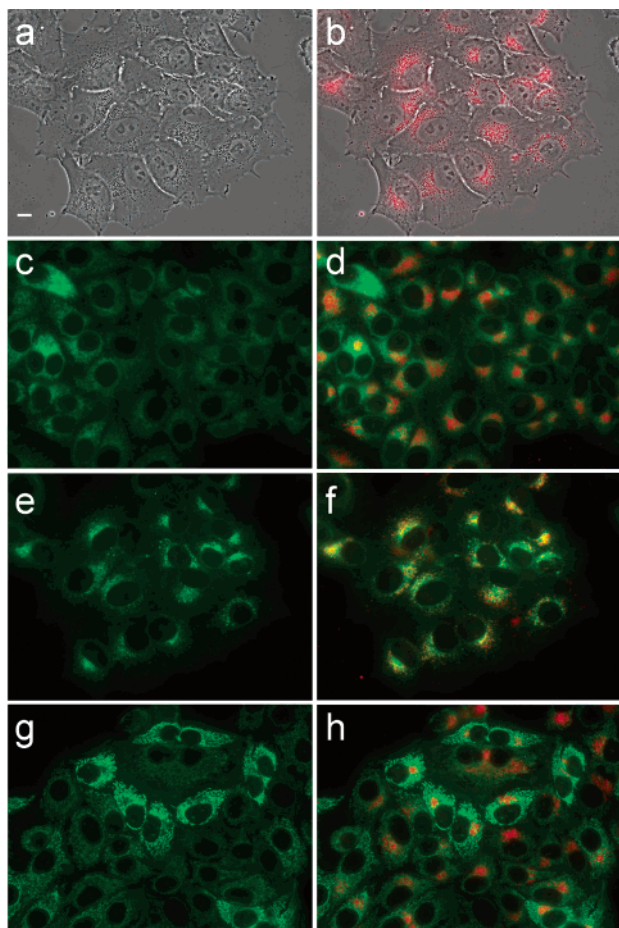
**Figure 5.** Subcellular localization of conjugate **10** in HEp2 cells at 10 $\mu$M for 18 h: (a) phase contrast, (b) overlay of **10** fluorescence and phase contrast, (c) DiOC$_6$ fluorescence, (d) overlay of DiOC$_6$ with **10** fluorescence, (e) LysoSensor Green fluorescence, (f) overlay of LysoSensor Green with **10** fluorescence, (g) MitoTracker Green fluorescence, (h) overlay of MitoTracker Green with **10** fluorescence. Scale bar: 10 $\mu$m.

fluorescent patterns observed for conjugates **4** and **10**, respectively, and their overlay with the organelle specific fluorescent probes LysoSensor Green (lysosomes), Mitotracker Green (mitochondria), and DiOC$_6$ (ER). Similar figures were obtained for conjugates **5**, **6**, and **11** (Supporting Information, Figures S8−S10). The preferential sites of intracellular localization were found to be the ER for conjugates **4**, **5**, and **6** and the lysosomes for **10** and **11**. These results indicate that the structure of the porphyrin ring and the overall molecule charge play an important role in determining the preferential sites of localization of these conjugates within cells. Although both conjugates **4** and **10** contain a NLS SV40 sequence, the cell nucleus is not their main localization site; it is possible, however, that in the case of **4** a small amount of conjugate localizes near or within the nucleus, thus explaining its higher phototoxicity compared with the other conjugates. A boronated porphyrin conjugated to a NLS has been recently reported, but there was no indication that it localizes in cell nuclei.[48] We hypothesize that multiple NLS sequences might be required in order to achieve preferential nuclear localization of porphyrin macrocycles. We have previously observed that porphyrin−peptide conjugates bearing 1−4 cationic amino acids localize preferentially in the lysosomes, probably as a result of an endocytic mechanism of uptake.[32] It is possible that while the carboxylic acid substituted conjugates **10** and **11** stay trapped in the lysosomes, which have a low internal pH, conjugates **4**, **5**, and **6** are delivered to the more

sensitive ER and consequently show higher phototoxicity. The ER is an important organelle that regulates protein synthesis, cellular responses to stress, and intracellular Ca$^{2+}$ levels; porphyrin-mediated ER stress can potentially lead to rapid cell death by apoptosis via activation of caspases, a family of cysteine-dependent proteases.[24,49,50]

## Conclusions

The biological efficacy of porphyrin sensitizers can potentially be increased by conjugation to a peptide that enhances their cellular uptake and delivery to sensitive intracellular compartments. Five new porphyrin−peptide conjugates bearing low molecular weight PEG linkers to the NLS SV40 or the fusogenic HIV-1 Tat 40−60 and octa-arginine peptide sequences were synthesized and characterized. CD studies indicate that these conjugates assume an extended (vs bent) conformation in aqueous solution at pH 7.5. The uptake of the conjugates by human HEp2 cells depends on the nature and sequence of the amino acid residues and on the substituents at the porphyrin periphery. Conjugates **4**−**6** were taken-up by cells to a higher extent than **10** and **11** and localized preferentially in the ER, whereas conjugates **10** and **11** were mainly found in the lysosomes. Among all conjugates studied, **6** accumulated the most within cells and **4** was the most phototoxic. The in vivo properties of the conjugates were not evaluated in this study and might or might not correlate with the in vitro findings. Our results show that the cellular uptake, phototoxicity, and preferential sites of subcellular localization of porphyrin−peptide conjugates depend on both the structure of the porphyrin and the nature of the peptide sequence.

**Supporting Information Available:** $^1$H NMR and $^{13}$C NMR for all compounds synthesized, traces from HPLC analysis for porphyrin conjugates, and fluorescence microscopy images for all conjugates. This material is available free of charge via the Internet at http://pubs.acs.org.

## References

(1) Dougherty, T. J.; Gomer, C. J.; Henderson, B. W.; Jori, G.; Kessel, D.; Korbelik, M.; Moan, J.; Peng, Q. Photodynamic therapy. *J. Natl. Cancer Inst.* **1998**, *90*, 889−905.

(2) Pandey, R. K.; Zheng, G. Porphyrins as photosensitizers in photodynamic therapy. In *The Porphyrin Handbook*; Kadish, K. M., Smith, K. M., Guilard, R., Eds.; Academic Press: Boston, MA, 2000; Vol. 6, pp 157−230.

(3) Soloway, A. H.; Tjarks, W.; Barnum, B. A.; Rong, F. G.; Barth, R. F.; Codogni, I. M.; Wilson, J. G. The chemistry of neutron capture therapy. *Chem. Rev.* **1998**, *98*, 1515−1562.

(4) Barth, R. F.; Coderre, J. A.; Vicente, M. G. H.; Blue, T. E. Boron neutron capture therapy of cancer: Current status and future prospects. *Clin. Cancer Res.* **2005**, *11*, 3987−4002.

(5) (a) Fairchild, R. G.; Bond, V. P. Current status of $^{10}$B neutron capture therapy: enhancement of tumor dose via beam filtration and dose rate, and the effects of these parameters on minimum boron content: a theoretical evaluation. *Int. J. Radiat. Oncol., Biol., Phys.* **1985**, *11*, 831−840. (b) Gabel, D.; Foster, S.; Fairchild, R. G. The Monte Carlo simulation of the biological effect of the $^{10}$B(n,$\alpha$)$^7$Li reaction in cells and tissue and its implication for boron neutron capture therapy. *Radiat. Res.* **1987**, *111*, 14−25.

(6) (a) Hartman, T.; Carlsson, J. Radiation dose heterogeneity in receptor and antigen mediated boron neutron capture therapy. *Radiother. Oncol.* **1994**, *31*, 61−75. (b) Hartman, T.; Lundqvist, H.; Westlin, J.-E.; Carlsson, J. Radiation doses to the cell nucleus in single cells and cells in micrometastases in targeted therapy with I-131 labeled ligands or antibodies. *Int. J. Radiat. Oncol., Biol., Phys.* **2000**, *46*, 1025−1036.

(7) (a) Hamblin, M. R.; Newman, E. L. Photosensitizer targeting in photodynamic therapy. I. Conjugates of haematoporphyrin with albumin and transferrin. *J. Photochem. Photobiol. B: Biol.* **1994**, *26*, 45−56. (b) Hamblin, M. R.; Newman, E. L. Photosensitizer targeting in photodynamic therapy. II. Conjugates of haematoporphyrin with serum lipoproteins. *J. Photochem. Photobiol. B: Biol.* **1994**, *26*, 147−157.

(8) Soini, A. E.; Yashunsky, D. V.; Meltola, N. J.; Ponomarev, G. V. Influence of linker unit on performance of palladium(II) coproporphyrin labelling reagent and its bioconjugates. *Luminescence* **2003**, *18*, 182−92.

(9) Chudinov, A. V.; Rumiantseva, V. D.; Lobanov, A. V.; Chudinova, G. K.; Stomakhin, A. A.; Mironov, A. F. Synthesis of conjugates of bovine serum albumin with water-soluble ytterbium porphyrins. *Bioorg. Khim.* **2004**, *30*, 99−104.

(10) Li, H.; Fedorova, O. S.; Trumble, W. R.; Fletcher, T. R.; Czuchajowski, L. Site-specific photomodification of DNA by porphyrin-oligonucleotide conjugates synthesized via a solid-phase H-phosphonate approach. *Bioconj. Chem.* **1997**, *8*, 49−56.

(11) (a) Mestre, B.; Jakobs, A.; Pratviel, G.; Meunier, B. Structure/nuclease activity relationships of DNA cleavers based on cationic metalloporphyrin-oligonucleotide conjugates. *Biochemistry* **1996**, *35*, 9140−9149. (b) Mestre, B.; Pitie, M.; Loup, C.; Claparols, C.; Pratviel, G.; Meunier, B. Influence of the nature of the porphyrin ligand on the nuclease activity of metalloporphyrin-oligonucleotide conjugates designed with cationic, hydrophobic or anionic metalloporphyrins. *Nucleic Acids Res.* **1997**, *25*, 1022−1027.

(12) Bedel-Cloutour, C. H.; Mauclaire, L.; Saux, A.; Pereyre, M. Syntheses of functionalized indium porphyrins for monoclonal antibody labeling. *Bioconj. Chem.* **1996**, *7*, 617−627.

(13) (a) Del Governatore, M.; Hamblin, M. R.; Piccinini, E. E.; Ugolini, G.; Hasan, T. Targeted photo-destruction of human colon cancer cells using charged 17.1A chlorin e$_6$ immunoconjugates. *Br. J. Cancer* **2000**, *82*, 56−64. (b) Hamblin, M. R.; Del Governatore, M.; Rizvi, I.; Hasan, T. Biodistribution of charged 17.1A photoimmunoconjugates in a murine model of hepatic metastasis of colorectal cancer. *Br. J. Cancer* **2000**, *83*, 1544−1551.

(14) Hudson, R.; Carcenac, M.; Smith, K.; Madden, L.; Clarke, O. J.; Pelegrin, A.; Greenman, J.; Boyle, R. W. The development and characterization of porphyrin isothiocyanate-monoclonal antibody conjugates for photoimmunotherapy. *Br. J. Cancer* **2005**, *92*, 1442−1449.

(15) Savitsky, A. A.; Gukasova, N. V.; Gumanov, S. G.; Feldman, N. B.; Luk'yanets, E. A.; Mironov, A. F.; Yakubovskaya, R. I.; Lutsenko, S. V.; Severin, S. E. Cytotoxic action of conjugates of alpha-fetoprotein and epidermal growth factor with photoheme, chlorines, and phthalocyanines. *Biochemistry (Moscow)* **2000**, *65*, 732−736.

(16) (a) Gijsens, A.; De Witte, P. Photocytotoxic action of EGF−PVA-Sn(IV)chlorin e$_6$ and EGF-dextran-Sn(IV)chlorin e$_6$ internalizable conjugates on A431 cells. *Int. J. Oncol.* **1998**, *13*, 1171−1177. (b) Gijsens, A.; Missiaen, L.; Merlevede, W.; de Witte, P. Epidermal growth factor-mediated targeting of chlorin e$_6$ selectively potentiates its photodynamic activity. *Cancer Res.* **2000**, *60*, 2197−2202.

(17) Chen, X.; Hui, L.; Foster, D. A.; Drain, C. M. Efficient synthesis and photodynamic activity of porphyrin-saccharide conjugates: targeting and incapacitating cancer cells. *Biochemistry* **2004**, *43*, 10918−10929.

(18) Li, G.; Pandey, S. K.; Graham, A.; Dobhal, M. P.; Mehta, R.; Chen, Y.; Gryshuk, A.; Rittenhouse-Olson, K.; Oseroff, A.; Pandey, R. K. Functionalization of OEP-based benzochlorins to develop carbohydrate-conjugated photosensitizers. Attempt to target beta-galactoside-recognized proteins. *J. Org. Chem.* **2004**, *69*, 158−172.

(19) (a) Soukos, N. S.; Hamblin, M. R.; Hasan, T. The effect of charge on cellular uptake and phototoxicity of polylysine chlorin(e$_6$) conjugates. *Photochem. Photobiol.* **1997**, *65*, 723−729. (b) Hamblin, M. R.; O'Donnell, D. A.; Murthy, N.; Rajagopalan, K.; Michaud, N.; Sherwood, M. E.; Hasan, T. Polycationic photosensitizer conjugates: effects of chain length and Gram classification on the photodynamic inactivation of bacteria. *J. Antimicrob. Chemother.* **2002**, *49*, 941−951.

(20) (a) Omelyanenko, V.; Gentry, C.; Kopeckova, P.; Kopecek, J. HPMA copolymer-anticancer drug-OV-TL16 antibody conjugates. II. Processing in epithelial ovarian carcinoma cells in vitro. *Int. J. Cancer* **1998**, *75*, 600−608. (b) Lu, J. M.; Peterson, C. M.; Guo-Shiah, J.; Gu, Z. W.; Peterson, C. A.; Straight, R. C.; Kopecek, J. Cooperativity between free and N−(2-hydroxypropyl) methacrylamide copolymer bound adriamycin and meso-chlorin e$_6$ monoethylene diamine induced photodynamic therapy in human epithelial ovarian carcinoma in vitro. *Int. J. Oncol.* **1999**, *15*, 5−16. (c) Tijerina, M.; Kopeckova, P.; Kopecek, J. Mechanisms of cytotoxicity in human ovarian carcinoma cells exposed to free Mce6 or HPMA copolymer-Mce6 conjugates. *Photochem. Photobiol.* **2003**, *77*, 645−652. (d) Tijerina, M.; Kopeckova, P.; Kopecek, J., Correlation of subcellular compartmentalization of HPMA copolymer-Mce6 conjugates with chemotherapeutic activity in human ovarian carcinoma cells. *Pharm. Res.* **2003**, *20*, 728−737.

(21) Rosenkranz, A. A.; Jans, D. A.; Sobolev, A. S. Targeted intracellular delivery of photosensitizers to enhance photodynamic efficiency. *Immunol. Cell Biol.* **2002**, *78*, 452−464.

(22) Hudson, R.; Boyle, R. W. Strategies for selective delivery of photodynamic sensitizers to biological targets. *J. Porphyrins Phthalocyanines* **2004**, *8*, 954−975.

(23) Osterloh, J.; Vicente, M. G. H. Mechanisms of porphyrinoid localization in tumors. *J. Porphyrins Phthalocyanines* **2002**, *6*, 305−324.

(24) Kessel, D. Correlation between subcellular localization and photodynamic efficacy. *J. Porphyrins Phthalocyanines* **2004**, *8*, 1009−1014.

(25) Kalderon, D.; Roberts, B. L.; Richardson, W. D.; Smith, A. E. A short amino acid sequence able to specify nuclear location. *Cell* **1984**, *39*, 499−509.

(26) Boulikas, T. Nuclear localization signals. *Crit. Rev. Eukariotic Gene Expression* **1993**, *3*, 193−227.

(27) Lombardo, E.; Ramirez, J. C.; Garcia, J.; Almendral, J. M. Complementary roles of multiple nuclear targeting signals in the capsid proteins of the parvovirus minute virus of mice during assembly and onset of the infection. *J. Virol.* **2002**, *76*, 7049−7059.

(28) (a) Lanford, R. E.; Butel, J. S. Construction and characterization of an SV40 mutant defective in nuclear transport of T antigen. *Cell* **1984**, *37*, 801−813. (b) Lanford, R. E.; Kanda, P.; Kennedy, R. C. Induction of nuclear transport with a synthetic peptide homologous to the SV40 T antigen transport signal. *Cell* **1986**, *46*, 575−582. (c) Feldherr, C. M.; Lanford, R. E.; Akin, D. Signal-mediated nuclear transport in simian virus 40-transformed cells is regulated by large tumor antigen. *Proc. Natl. Acad. Sci. U.S.A.* **1992**, *89*, 11002−11005.

(29) (a) Sobolev, A. S.; Akhlynina, T. V.; Yachmenev, S. V.; Rosenkranz, A. A.; Severin, E. S. Internalizable insulin-BSA-chlorin e$_6$ conjugate is a more effective photosensitizer than chlorin e$_6$ alone. *Biochem. Int.* **1992**, *26*, 445−450. (b) Akhlynina, T. V.; Rosenkranz, A. A.; Jans, D. A.; Gulak, P. V.; Serebryakova, N. V.; Sobolev, A. S. The use of internalizable derivatives of chlorin e$_6$ for increasing its photosensitizing activity. *Photochem. Photobiol.* **1993**, *58*, 45−48. (c) Akhlynina, T. V.; Jans, D. A.; Rosenkranz, A. A.; Statsyuk, N. V.; Balashova, I. Y.; Toth, G.; Pavo, I.; Rubin, A. B.; Sobolev, A. S. Nuclear targeting of chlorin e$_6$ enhances its photosensitizing activity. *J. Biol. Chem.* **1997**, *272*, 20328−20331. (d) Akhlynina, T. V.; Jans, D. A.; Statsyuk, N. V.; Balashova, I. Y.; Toth, G.; Pavo, I.; Rosenkranz, A. A.; Naroditsky, B. S.; Sobolev, A. S. Adenoviruses synergize with nuclear localization signals to enhance nuclear delivery and photodynamic action of internalizable conjugates containing chlorin e$_6$. *Int. J. Cancer* **1999**, *81*, 734−740.

(30) Chaloin, L.; Bigey, P.; Loup, C.; Marin, M.; Galeotti, N.; Piechaczyk, M.; Heitz, F.; Meunier, B. Improvement of porphyrin cellular delivery and activity by conjugation to a carrier peptide. *Bioconj. Chem.* **2001**, *12*, 691−700.

(31) Bisland, S. K.; Singh, D.; Gariepy, J. Potentiation of chlorine e$_6$ photodynamic activity in vitro with peptide-based intracellular vehicles. *Bioconj. Chem.* **1999**, *10*, 982−992.

(32) Sibrian-Vazquez, M.; Jensen, T. J.; Fronczek, F. R.; Hammer, R. P.; Vicente, M. G. H. Synthesis and characterization of positively charged porphyrin-peptide conjugates. *Bioconj. Chem.* **2005**, *16*, 852−863.

(33) (a) Schwartz, J. J.; Zhang, S. Peptide-mediated cellular delivery. *Curr. Opin. Mol. Ther.* **2000**, *2*, 162−167. (b) Lundberg, P.; Langel, U. A brief introduction to cell-penetrating peptides. *J. Mol. Recognit.* **2003**, *16*, 227−233. (c) Richard, J. P.; Melikov, K.; Vives, E.; Ramos, C.; Verbeure, B.; Gait, M. J.; Chernomordik, L. V.; Lebleu, B. Cell-penetrating peptides: a reevaluation of the mechanism of cellular uptake. *J. Biol. Chem.* **2003**, *278*, 585−590. (d) Futaki, S.; Goto, S.; Suzuki, T.; Nakase, I.; Sugiura, Y. Structural variety of membrane permeable peptides. *Curr. Protein Pept. Sci.* **2003**, *4*, 87−96.

(34) Derossi, D.; Joliot, A.; Chassaing, G.; Prochiantz, A. The third helix of the Antennapedia homeodomain translocates through biological membranes. *J. Biol. Chem.* **1994**, *269*, 10444−10450.

(35) Vives, E. Cellular uptake of the Tat peptide: an endocytosis mechanism following ionic interactions. *J. Mol. Recognit.* **2003**, *16*, 265−271.

(36) (a) Normand, N.; van Leeuwen, H.; O'Hare, P. Particle formation by the HSV protein VP22 enabling protein and nucleic acid delivery. *J. Biol. Chem.* **2001**, *276*, 15042−15050. (b) Brewis, N. D.; Phelan, A.; Normand, N.; Choolun, E.; O'Hare, P. Particle assembly incorporating a VP22-BH3 fusion protein, facilitating intracellular delivery, regulated release, and apoptosis 1. *Mol. Ther.* **2003**, *7*, 262−270.

(37) (a) Mitchell, D. J.; Kim, D. T.; Steinman, L.; Fathman, C. G.; Rothbard, J. B. Polyarginine enters cells more efficiently than other polycationic homopolymers. *J. Pept. Res.* **2000**, *56*, 318−325. (b) Rothbard, J. B.; Jessop, T. C.; Lewis, R. S.; Murray, B. A.; Wender, P. A. Role of membrane potential and hydrogen bonding in the mechanism of translocation of guanidinium-rich peptides into cells. *J. Am. Chem. Soc.* **2004**, *126*, 9506−9507.

(38) (a) Rothbard, J. B.; Garlington, S.; Lin, Q.; Kirschberg, T.; Kreider, E.; McGrane, P. L.; Wender, P. A.; Khavari, P. A. Conjugation of arginine oligomers to cyclosporin A facilitates topical delivery and inhibition of inflammation. *Nat. Med.* **2000**, *6*, 1253−1257. (b) Futaki, S.; Ohashi, W.; Suzuki, T.; Niwa, M.; Tanaka, S.; Ueda, K.; Harashima, H.; Sugiura, Y. Stearylated arginine-rich peptides: A new class of transfection systems. *Bioconj. Chem.* **2001**, *12*, 1005−1011. (c) Kirschberg, T. A.; VanDeusen, C. L.; Rothbard, J. B.; Yang, M.; Wender, P. A. Arginine-based molecular transporters: The synthesis and chemical evaluation of releasable taxol-transporter conjugates. *Org. Lett.* **2003**, *5*, 3459−3462.

(39) (a) Greenwald, R. B. PEG drugs: an overview. *J. Controlled Release* **2001**, *74*, 159−171. (b) Greenwald, R. B.; Choe, Y. H.; McGuire, J.; Conover, C. D. Effective drug delivery by PEGylated drug conjugates. *Adv. Drug Delivery Rev.* **2003**, *55*, 217−250.

(40) (a) Hamblin, M. R.; Miller, J. L.; Rizvi, I.; Ortel, B.; Maytin, E. V.; Hasan, T. Pegylation of a chlorin e$_6$ polymer conjugate increases tumor targeting of photosensitizer. *Cancer Res.* **2001**, *61*, 7155−7162. (b) Kim, Y. S.; Song, R.; Hyun Kim, D.; Jun, M. J.; Sohn, Y. S. Synthesis, biodistribution and antitumor activity of hematopor-phyrin-platinum(II) conjugates. *Bioorg. Med. Chem.* **2003**, *11*, 1753−1760.

(41) (a) Lottner, C.; Bart, K. C.; Bernhardt, G.; Brunner, H. Soluble tetraarylporphyrin-platinum conjugates as cytotoxic and phototoxic antitumor agents. *J. Med. Chem.* **2002**, *45*, 2079−2089. (b) Lottner, C.; Bart, K. C.; Bernhardt, G.; Brunner, H. Hematoporphyrin-derived soluble porphyrin-platinum conjugates with combined cytotoxic and phototoxic antitumor activity. *J. Med. Chem.* **2002**, *45*, 2064−2078. (c) Lottner, C.; Knuechel, R.; Bernhardt, G.; Brunner, H. Combined chemotherapeutic and photodynamic treatment on human bladder cells by hematoporphyrin-platinum(II) conjugates. *Cancer Lett.* **2004**, *203*, 171−180.

(42) Nori, A.; Kopecek, J. Intracellular targeting of polymer-bound drugs for cancer chemotherapy. *Adv. Drug Delivery Rev.* **2005**, *57*, 609−636.

(43) (a) Suedhem, S.; Hollander, S.; Shi, J.; Konradsson, P.; Liedberg, B.; Svensson, S. C. T. Synthesis of a series of oligo(ethyleneglycol)-terminated alkanethiol amides designed to address structural and stability of biosensing interfaces. *J. Org. Chem.* **2001**, *66*, 4494−4503. (b) Wosnick, J. H.; Charlene M.; Mello, C. M.; Swager, T. M. Synthesis and application of poly(phenylene ethynylene)s for bioconjugation: A conjugated polymer-based fluorogenic probe for proteases. *J. Am. Chem. Soc.* **2005**, *127*, 3400−3405.

(44) Luguya, R.; Jaquinod, L.; Fronczek, F. R.; Vicente, M. G. H.; Smith, K. M. Synthesis and reactions of meso-(*p*-nitrophenyl)porphyrins. *Tetrahedron* **2004**, *60*, 2757−2763.

(45) Greenfield, N.; Fasman, G. D. Computed circular dichroism spectra for the evaluation of protein conformation. *Biochemistry* **1969**, *8*, 4108−4116.

(46) Conti, E.; Uy, M.; Leighton, L.; Blobel, G.; Kuriyan, J. Crystal-lographic analysis of the recognition of a nuclear localization signal by the nuclear import facto kariopherin α. *Cell* **1988**, *94*, 193−204.

(47) Loret, E. P.; Vives, E.; Pui Shing Ho, P. S.; Rochat, H.; Van Rietschoten, J.; Johnson, W. C., Jr. Activating region of HIV-1 Tat protein: vacuum UV circular dichroism and energy minimization. *Biochemistry* **1991**, *30*, 6013−6023.

(48) Dozzo, P.; Koo, M.-S.; Berger, S.; Forte, T. M.; Kahl, S. B. Synthesis, characterization, and plasma lipoprotein association of a nucleus-targeted boronated porphyrin. *J. Med. Chem.* **2005**, *48*, 357−359.

(49) Groenendyk, J.; Michalak, M. Endoplasmic reticulum quality control and apotosis. *Acta Biochim. Pol.* **2005**, *52*, 381−395.

(50) Rao, R. V.; Hermel, E.; Castro-Obregon, S.; del Rio, G.; Ellerby, L. M.; Ellerby, H. M.; Bredesen, D. E. Coupling endoplasmic reticulum stress to the cell death program. Mechanism of caspase activation. *J. Biol. Chem.* **2001**, *276*, 33869−33874.